GLP-1 Receptor Activation Indirectly Reduces Hepatic Lipid Accumulation But Does Not Attenuate Development of Atherosclerosis in Diabetic Male *ApoE*$^{-/-}$ Mice

Naim Panjwani, Erin E. Mulvihill, Christine Longuet, Bernardo Yusta, Jonathan E. Campbell, Theodore J. Brown, Catherine Streutker, Dianne Holland, Xiemin Cao, Laurie L. Baggio, and Daniel J. Drucker

Departments of Medicine (N.P., E.E.M., C.L., B.Y., J.E.C., D.H., X.C., L.L.B., D.J.D.), and Physiology (T.J.B.) Samuel Lunenfeld Research Institute, Mt. Sinai Hospital, Toronto Ontario Canada M5G 1X5; and the Department of Laboratory Medicine (C.S.), St. Michael's Hospital, University of Toronto, Toronto, Ontario, Canada M5B 1W8

Glucagon-like peptide-1 receptor (GLP-1R) agonists reduce lipid accumulation in peripheral tissues, attenuating atherosclerosis and hepatic steatosis in preclinical studies. We examined whether GLP-1R activation decreases atherosclerosis progression in high-fat diet-fed male *ApoE*$^{-/-}$ mice after administration of streptozotocin and treatment with the long-acting GLP-1R agonist taspoglutide administered once monthly *vs.* metformin in the drinking water for 12 wk. Taspoglutide did not reduce plaque area or lipid content in the aortic arch or abdominal aorta, and no significant change in aortic macrophage accumulation was detected after taspoglutide or metformin. In contrast, hepatic triglyceride levels were significantly reduced in livers from taspoglutide-treated mice. Both peripheral and intracerebroventricular administration of exendin-4 rapidly decreased plasma triglyceride levels in fasted mice, and taspoglutide therapy in *ApoE*$^{-/-}$ mice modulated the expression of hepatic genes controlling fatty acid uptake and oxidation. We were unable to detect expression of the entire *Glp1r* coding sequence in macrophages isolated from *ApoE*$^{-/-}$, C57BL/6, and *IL10*$^{-/-}$ mice. Similarly, *Glp1r* mRNA transcripts were not detected in RNA from isolated murine hepatocytes. Using Western blotting and tissue extracts from *Glp1r*$^{+/+}$ and *Glp1r*$^{-/-}$ mice, and cells transfected with a tagged murine GLP-1R cDNA, we could not validate the sensitivity and specificity of three different GLP-1R antisera commonly used for the detection of GLP-1R protein. Taken together, these findings illustrate divergent actions of GLP-1R agonists on atherosclerosis progression and accumulation of ectopic lipid in *ApoE*$^{-/-}$ mice and highlight the importance of indirect GLP-1R actions for the control of hepatic lipid accumulation. **(*Endocrinology* 154: 127–139, 2013)**

There are now multiple classes of antidiabetic medications used for the treatment of type 2 diabetes (1). All of these drugs were approved based on their ability to lower blood glucose; however, the mechanisms activated by distinct antidiabetic agents vary widely. Two of the relatively newer classes, glucagon-like peptide-1 receptor (GLP-1R) agonists and dipeptidyl peptidase-4 (DPP-4) inhibitors, exert their glucose-lowering actions predominantly through activation of the GLP-1R (2). Although classical islet actions of GLP-1 include stimulation of insulin and inhibition of glucagon secretion, GLP-1Rs are widely distributed on blood vessels and cardiomy-

ISSN Print 0013-7227 ISSN Online 1945-7170
Printed in U.S.A.

doi: 10.1210/en.2012-1937 Received September 11, 2012. Accepted October 16, 2012.
First Published Online November 26, 2012

For editorial see page 4

Abbreviations: DPP-4, Dipeptidyl peptidase-4; FACS, fluorescence-activated cell sorting; GLP-1R, glucagon-like peptide-1 receptor; LXR, liver X receptor; OGTT, oral glucose tolerance test; STZ, streptozotocin.

ocytes and exert direct effects in the cardiovascular system (3). Activation of the GLP-1R also reduces blood pressure, decreases intestinal lipoprotein secretion, and attenuates inflammation, actions that might predict a favorable reduction in the development of atherosclerosis (4, 5).

There are no completed long-term prospective clinical studies that address whether sustained GLP-1R activation modifies the risk of developing atherosclerosis, strokes, or heart attacks in diabetic individuals (6). The actions of incretin-based therapies have been examined in short-term studies of genetically modified rodents at high risk for development of atherosclerosis. Both GLP-1R agonists and DPP-4 inhibitors reduce lesion formation and monocyte or macrophage accumulation in the aorta of $ApoE^{-/-}$ mice (7-10); however, the majority of these experiments have been carried out in nondiabetic mice for short periods of time.

Although hyperglycemia and insulin resistance substantially accelerate the development of clinical and experimental atherosclerosis (11), whether sustained activation of GLP-1R signaling might attenuate the development of atherosclerosis in the setting of insulin resistance, impairment of β-cell function, and hyperglycemia remains uncertain. We have now studied atherosclerosis progression in an established model of type 2 diabetes characterized by a combination of insulin resistance and β-cell dysfunction in high-fat fed mice administered the β-cell toxin streptozotocin (STZ) (12, 13), followed by continuous treatment with the long-acting GLP-1R agonist taspoglutide for 12 wk. We also examined the expression of the GLP-1R in cell types important for control of ectopic lipid deposition, principally macrophages and hepatocytes. Our findings raise new questions about the mechanisms through which GLP-1R agonists attenuate the development of fatty liver and atherosclerosis in mice.

Materials and Methods

Animals

All experimental procedures on animals conformed to the guidelines and policies approved by the Mount Sinai Hospital Animal Care Committee. Mice were maintained on a 12-h light (0700 h), 12-h dark (1900 h) cycle in a specific pathogen-free environment and had *ad libitum* access to food and water, except where noted. Four-week-old male $ApoE^{-/-}$ mice from The Jackson Laboratory (Bar Harbor, ME) were started on a high-fat (45% kcal) diet (D12451; Research Diets, New Brunswick, NJ). Modest hyperglycemia was induced using STZ (an initial dose of 75 mg/kg followed by a second dose of 125 mg/kg 10 d later), and mice with glucose levels from 15-25 mM were then randomized to different groups and treated for 12 wk with a once-monthly sc 0.4-mg taspoglutide microtablet suspension, a sc placebo microtablet, or metformin (400 mg/kg·d) continuously provided in the drinking water plus a sc placebo microtablet, as described in Supplemental Fig. 1 (published on The Endocrine Society's Journals Online web site at http://endo.endojournals.org). The STZ dosing regimen was based on pilot experiments and chosen to produce modest hyperglycemia, but not complete β-cell destruction. Preliminary dose-response experiments in mice verified that this dose of taspoglutide produced continuously elevated circulating levels of immunoreactive taspoglutide and effective glucose control without marked weight loss; the dose of metformin was based on dose-ranging pilot studies in $ApoE^{-/-}$ mice and on previous studies (13, 14). For isolation of tissues and cells for RNA analysis, C57BL/6, $IL\text{-}10^{-/-}$ (The Jackson Laboratory), $Gipr^{-/-}$, and $Glp1r^{-/-}$ mice (15) were maintained on regular animal chow.

Body composition

Total body fat and lean mass were measured using a mouse whole-body magnetic resonance analyzer (Echo Medical Systems, Houston, TX) after 5 and 10 wk of treatment as described (16). Food intake was measured and stool samples collected 3 d before euthanasia using single cages without bedding and preweighed food. On the last day, food and stool weights were recorded.

Oral glucose tolerance tests (OGTTs)

OGTTs were carried out after a 6-h fast (0700-1300 h). Glucose (1.5 mg/g body weight) was administered orally through a gavage tube, and blood glucose levels were measured by the glucose oxidase method using the Contour glucometer (Bayer Healthcare, Toronto, Ontario, Canada). For plasma insulin determinations, blood samples (50 μl) were drawn from the tail vein in a heparinized tube. Blood was mixed with 10% (vol/vol) TED (500,000 IU/ml Trasylol, 1.2 mg/ml EDTA, and 0.1 mM diprotin A) and plasma separated by centrifugation at 4 C and stored at −80 C until assayed using a mouse insulin ELISA (Alpco, Salem, NH).

Macrophage, adipocyte, and hepatocyte isolation

Cells and tissues were obtained from 10- to 14-wk-old male mice, with the exception of $ApoE^{-/-}$ mice (20 wk). To collect activated macrophages, mice were injected with 2 ml 4% thioglycolate 5 d before peritoneal extraction. Peritoneal cells were either immediately harvested for RNA, plated for 1 h in a six-well tissue culture plate, or subjected to fluorescence-activated cell sorting (FACS). For FACS purification, macrophages were identified as positive for both F4/80 (eBioscience, San Diego, CA, catalog item 12-4801) and CD11b (eBioscience, catalog item 17-0112). Adipose tissue macrophages were collected after collagenase digestion of adipose tissue, and FACS was used to isolate cells from the stromal vascular fraction, using F4/80 and CD11b as positive markers. Hepatocytes and the nonhepatocyte fraction (17) and adipocytes and the stromal vascular fraction were separated as described (18).

RT-PCR analysis

Mouse *Glp1r* mRNA analysis was performed as described (19). The mouse *Glp1r* transcript was amplified by PCR using primer pairs 5′-GTACCACGGTGTCCCTCTCA-3′ and 5′-CCTGTGTCCTTCACCTTCCCTA-3′, resulting in generation

of a PCR product encompassing the majority of the GLP-1R open reading frame and nucleotides within the 3′-untranslated and 3′-flanking region. After gel electrophoresis and transfer to membranes, blots were hybridized with a ^{32}P-labeled (5′-GGATGGGCTCCTCTCCTATC-3′) GLP-1R oligonucleotide. β-Actin RNA analysis by PCR was performed using primer pairs 5′-TGACATCCGTAAAGA-3′ and 3′-CAGCTCAGTAACAGTCC-5′. For analysis of gene expression in liver (Supplemental Table 1), cDNA from whole liver was subjected to real-time PCR analysis using the TaqMan real-time PCR gene expression assay (Applied Biosystems, Foster City, CA), with *Ppia* used as the internal control gene. *Glp1r* cDNA was cloned from *Glp1r*$^{-/-}$ lung and intestine into a TA cloning vector, sequenced, and subcloned into pcDNA3.1/myc-His(−) (Invitrogen Canada, Burlington, Ontario, Canada) for transfection into BHK fibroblasts as described below.

Detection of GLP-1R protein by Western blotting

Whole tissue extracts from mouse lung and BHK cell lysates were prepared by homogenization in RIPA buffer (1% Nonidet P-40, 0.5% sodium deoxycholate, and 0.1% sodium dodecyl sulfate in PBS) supplemented with protease inhibitor cocktail (Sigma-Aldrich, Oakville, Ontario, Canada). Thirty to forty micrograms of protein were resolved by SDS-PAGE and immunoblotted as described (20). Immunoprecipitations were performed using the ImmunoCruz IP/WB Optima F System (Santa Cruz Biotechnology, Santa Cruz, CA), Protein A Plus Agarose (Thermo Scientific, Rockford, IL), or Sepharose-conjugated anti-Myc-Tag (9B11) mouse monoclonal antibody (Cell Signaling Technology, Beverly, MA). Immune complexes were resolved by SDS-PAGE and analyzed by immunoblotting. The following rabbit polyclonal antibodies to the GLP-1R were used: sc-66911 (Santa Cruz Biotechnology), LS-A1205 (LifeSpan Biosciences, Seattle, WA), and ab39072 (Abcam, Cambridge, MA). The rabbit polyclonal anti-His-Tag antibody was from Cell Signaling Technology, and the mouse monoclonal anti-c-myc (9E10) antibody was from Santa Cruz. Transient transfection of BHK cells with 1) the murine *Glp1r*$^{+/+}$ cDNA or 2) the *Glp1r*$^{-/-}$ lung cDNA (long form; see Fig. 7) cloned into pcDNA3.1/myc-His(−) or 3) the empty vector was done using Lipofectamine 2000 reagent (Invitrogen) according to the manufacturer's protocol.

Plasma triglycerides in response to peripheral or intracerebroventricular exendin-4

C57BL/6 male mice, 8 wk of age, were placed on a high-fat (45% kcal) diet for 4 wk, then fasted overnight. On the day of the experiments, a blood sample was collected via the tail vein, and mice were injected with exendin-4 or saline either ip or via a stereotaxic intracerebroventricular injection as described (21, 22). Immediately after exendin-4 or vehicle administration, mice were injected iv with Triton WR1339 to block triglyceride clearance (0.5 mg/kg body weight, 15% solution prepared in saline). Blood samples were collected 1, 2, and 3 h after Triton WR1339 injection and centrifuged for 5 min at 6000 rpm, and plasma triglyceride levels were determined enzymatically (23).

Lipid tolerance test

After 6 wk of treatment with placebo, metformin, or taspoglutide, *ApoE*$^{-/-}$ mice were fasted overnight (1900-0900 h), and a lipid tolerance test was carried out as described (23).

Plasma cholesterol and adipokines

Blood (50 μl) was withdrawn from fasted *ApoE*$^{-/-}$ mice (1900-0900 h), mixed with 10% (vol/vol) TED (500,000 IU/ml Trasylol, 1.2 mg/ml EDTA, and 0.1 mM diprotin A), and plasma was separated by centrifugation at 4 C and stored at −80 C. Plasma was assayed for cholesterol using an enzymatic colorimetric assay kit (Wako, Richmond, VA, catalog item 439-17501). The Milliplex MAP Mouse Serum Adipokine Kit (EMD Millipore, Billerica, MA, MADPK-71K) was used to measure plasma levels of leptin, IL-6, resistin, TNF-α, and monocyte chemotactic protein-1.

Mean arterial pressure

Arterial pressure was measured from 1030-1530 h in trained awake *ApoE*$^{-/-}$ mice using an automated tail cuff system (BP-2000; Visitech Systems, Apex, NC) after 11 wk of treatment.

Histological analysis

The aortic root was isolated for quantification of atherosclerosis lesion size as described (24). ImageScope software version 11.0.2.716 (Aperio, Vista, CA) was used to quantify plaque area and lipids. The 15th and 20th aortic sections were stained with MAC-2 primary antibody (Cedarlane Laboratories, Burlington, Ontario, Canada) and visualized with diaminobenzidine. The liver embedded in OCT was cut and stained with hematoxylin and eosin and Oil-Red O. Histological sections were scored for hepatic lobular inflammation, ballooning, apoptosis, Kupffer cells, fibrosis, and steatosis according to guidelines set by the Pathology Committee of the NASH (nonalcoholic steatohepatitis) Clinical Research Network (25) in a blinded manner by a trained pathologist (C.S.).

Statistics

Results are presented as mean ± SE. Statistical analyses were done using repeated-measures ANOVA followed by Bonferroni's *post hoc* test. A P value < 0.05 was considered to be statistically significant. Sample size calculations were approximated using GraphPad StatMate version 2.00 software. The largest SD and a power of 80% were chosen to estimate the required sample size (n) per treatment group. The effect size was estimated from the mean difference observed between controls and taspoglutide-treated mice.

Results

Taspoglutide treatment of *ApoE*$^{-/-}$ mice

The results of previous studies demonstrated that continuous GLP-1 or exendin-4 administration attenuated the development of atherosclerosis in normoglycemic *ApoE*$^{-/-}$ mice (7, 10). Accordingly, we carried out experiments to assess the consequences of GLP-1R activation in hyperglycemic *ApoE*$^{-/-}$ mice employing the long-acting GLP-1R agonist taspoglutide (26) *vs.* the commonly used antidiabetic agent metformin, employed as a control for actions that might simply reflect improved glucoregulation (Supplemental Fig. 1). Taspoglutide significantly de-

creased food intake and body weight (Fig. 1, A and B). There were no significant differences in percent fat mass (Fig. 1C) or blood pressure (Supplemental Fig. 2A); epididymal white adipose tissue was lower in taspoglutide-treated mice, but the difference was not significant (Fig. 1D). Blood glucose levels remained elevated (~15 mM) even 2 h after glucose loading during an OGTT in placebo- and metformin-treated mice (Fig. 1E). In contrast, taspoglutide-treated mice exhibited significantly improved oral glucose tolerance (Fig. 1E) and an increased insulin to glucose ratio (Fig. 1F). Hemoglobin A1c levels were lower in taspoglutide-treated mice, but the difference was not statistically significant ($P = 0.19$) (Fig. 1G). Plasma levels of IL-6 were significantly reduced in $ApoE^{-/-}$ mice treated with metformin or taspoglutide, leptin levels were unchanged, and plasma resistin was increased in taspoglutide- *vs.* metformin-treated mice (Fig. 1, H–J). No significant changes in lipid tolerance as assessed by changes in plasma triglycerides after olive oil loading, fasting plasma cholesterol or triglycerides, or fecal cholesterol were detected across treatment groups, however fecal triglycerides were higher in the taspoglutide-treated mice (Supplemental Fig. 2).

Taspoglutide-treated $ApoE^{-/-}$ mice exhibited significantly increased plaque area in the aortic sinus compared with metformin-treated mice (Fig. 2, A and F). Intraplaque lipid was significantly reduced in metformin-treated mice but unchanged after taspoglutide administration (Fig. 2B). Total macrophage area was not different across treatment groups in the aortic sinus (Fig. 2C) or in the aortic arch (Fig. 2, D and G). Neither metformin nor taspoglutide significantly reduced plaque area in the abdominal aorta (Fig. 2, E and H).

The failure of taspoglutide to reduce aortic plaque area in hyperglycemic $ApoE^{-/-}$ mice differs from results obtained with GLP-1R agonists in previous studies of $ApoE^{-/-}$ mice (7, 10). Accordingly, we next examined the consequences of taspoglutide therapy on the liver, an organ that is also highly susceptible to ectopic lipid deposition and responsive to therapy with GLP-1R agonists in clinical and experimental models of diabetes (27-29). Liv-

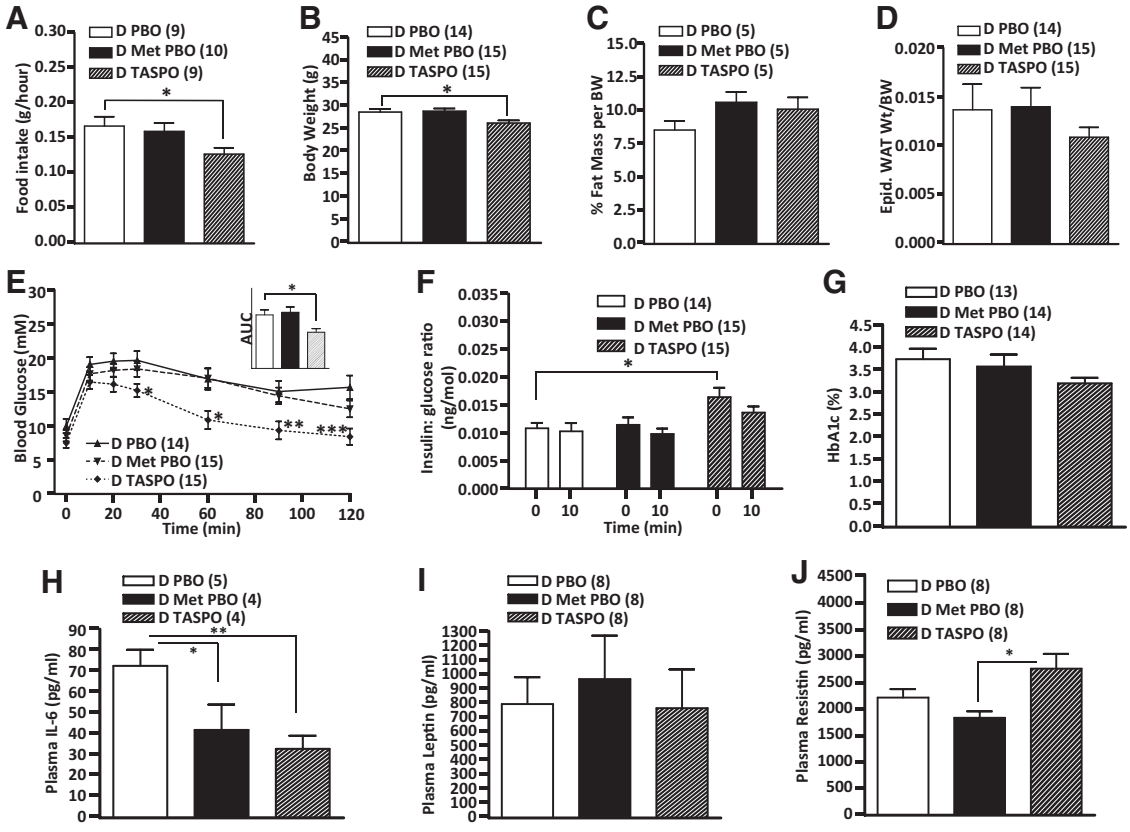

FIG. 1. Metabolic parameters in diabetic $ApoE^{-/-}$ mice treated with metformin or taspoglutide. Food intake (panel A), body weight (panel B), fat mass (panel C), epididymal white adipose tissue (Epid. WAT) (panel D), oral glucose tolerance (panel E), insulin to glucose ratios (panel F), hemoglobin A1c (panel G), plasma IL-6 (panel H), leptin (panel I), and resistin (panel J) at different time points (Supplemental Fig. 1) of treatment of diabetic (D) $ApoE^{-/-}$ with placebo (PBO), metformin (Met), or taspoglutide (TASPO). BW, Body weight. *, $P < 0.05$; **, $P < 0.01$; ***, $P < 0.001$ *vs.* placebo or indicated groups. Comparison between groups was made by one-way or two way ANOVA. The area under the glucose curve after the OGTT in placebo-treated mice on the high-fat diet after STZ treatment was significantly greater than the area under the glucose curve obtained during an OGTT in age-matched $ApoE^{-/-}$ mice on a high-fat diet but not treated with STZ (data not shown). The numbers in parentheses denote the number of replicates per experimental condition.

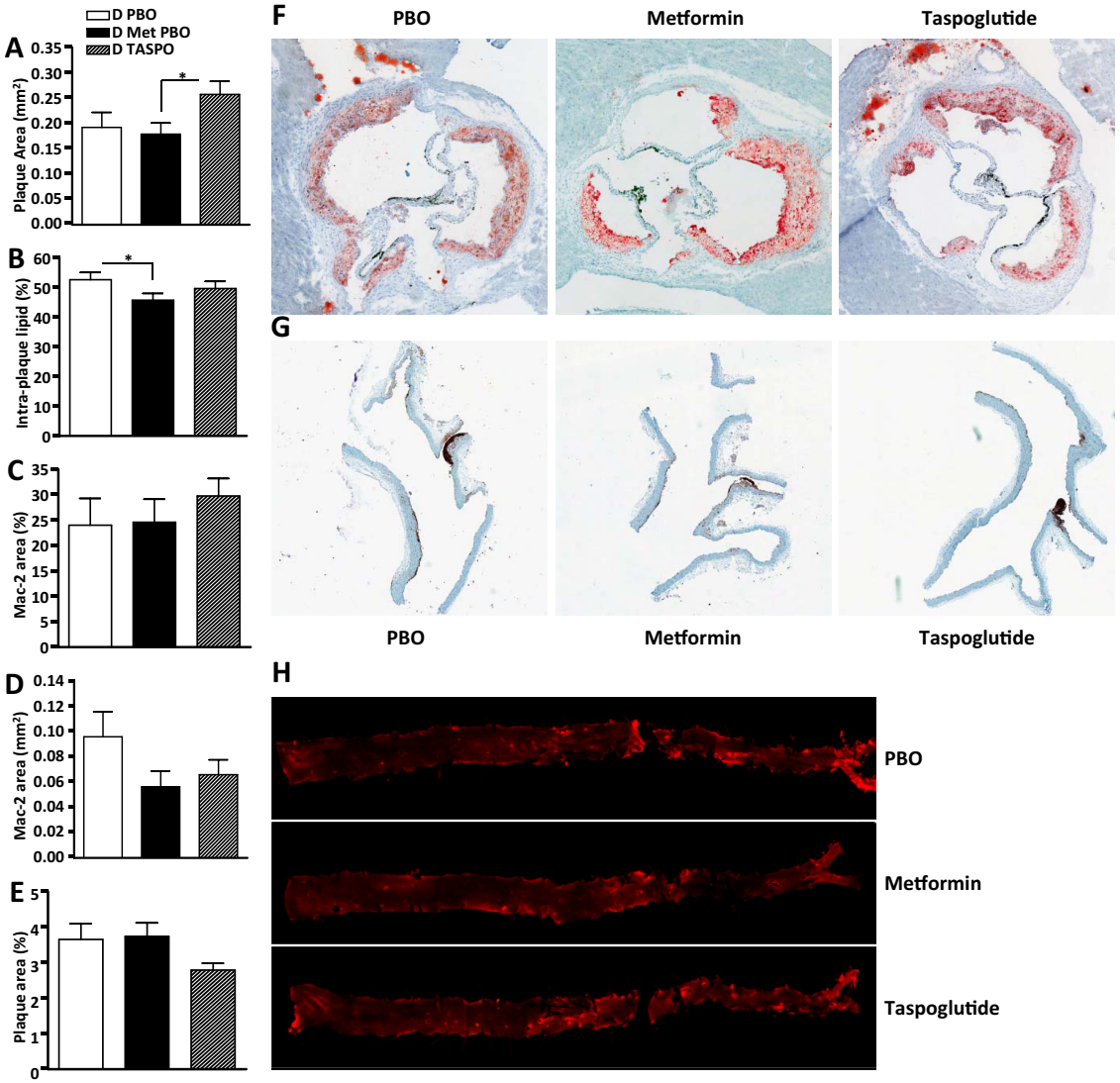

FIG. 2. Neither taspoglutide nor metformin modifies atherosclerotic plaque development or aortic macrophage accumulation in diabetic *ApoE*$^{-/-}$ mice. Plaque area (panel A), intraplaque lipid assessed by Oil-Red O staining (panel B), quantification of Mac-2 staining for macrophages in plaques at the aortic sinus and aortic arch (panels C and D), atherosclerotic plaque area in the descending aorta (panel E), aortic sections stained with Oil-Red O (magnification, ×5) (panel F), aortic macrophage accumulation in sections stained with anti-Mac2 antibody, Magnification, ×5 (panel G), and *en face* lipid staining of the descending aorta (panel H) in diabetic (D) *ApoE*$^{-/-}$ mice treated with placebo (PBO), metformin (Met), or taspoglutide (TASPO) for 12 wk. *, $P < 0.05$, comparison between groups was made by one-way or two way ANOVA.

ers from diabetic mice treated with taspoglutide weighed significantly less compared with livers from metformin-treated mice (Fig. 3A); however, parameters of liver injury were similar in control *vs.* metformin- or taspoglutide-treated mice (Supplemental Fig. 3). Livers from mice treated with taspoglutide appeared healthier with no gross nodular enlargement and exhibited significantly reduced levels of triglycerides and cholesterol (Fig. 3, B–D). Cholesterol and triglyceride levels in stools were not significantly different among the three groups (Supplemental Fig. 2, E and F).

We next explored mechanisms through which GLP-1R agonists modify hepatic lipid accumulation. Because acute intracerebroventricular exendin-4 administration reduced hepatic triglyceride levels in mice under hyperinsulinemic-euglycemic clamp conditions (30), we assessed hepatic lipid secretion in high-fat-fed mice. Acute peripheral or intracerebroventricular administration of exendin-4 rapidly reduced plasma triglyceride levels in fasted mice after 4 wk of high-fat feeding, demonstrating that GLP-1R activation leads to reduction rather than stimulation of hepatocyte triglyceride secretion in the absence of hyperinsulinemia (Fig. 4, A and B).

Analysis of gene expression profiles for mRNA transcripts encoding proteins involved in the regulation of cholesterol, free fatty acid, and triglyceride metabolism is shown in Fig. 5 and Supplemental Table 2. Taspoglutide treatment significantly increased levels of mRNA transcripts for the transcription factor liver X receptor (*Lxr*) as well as multiple LXR target genes, *Abca1*, *Abcg5*, *Abcg1*,

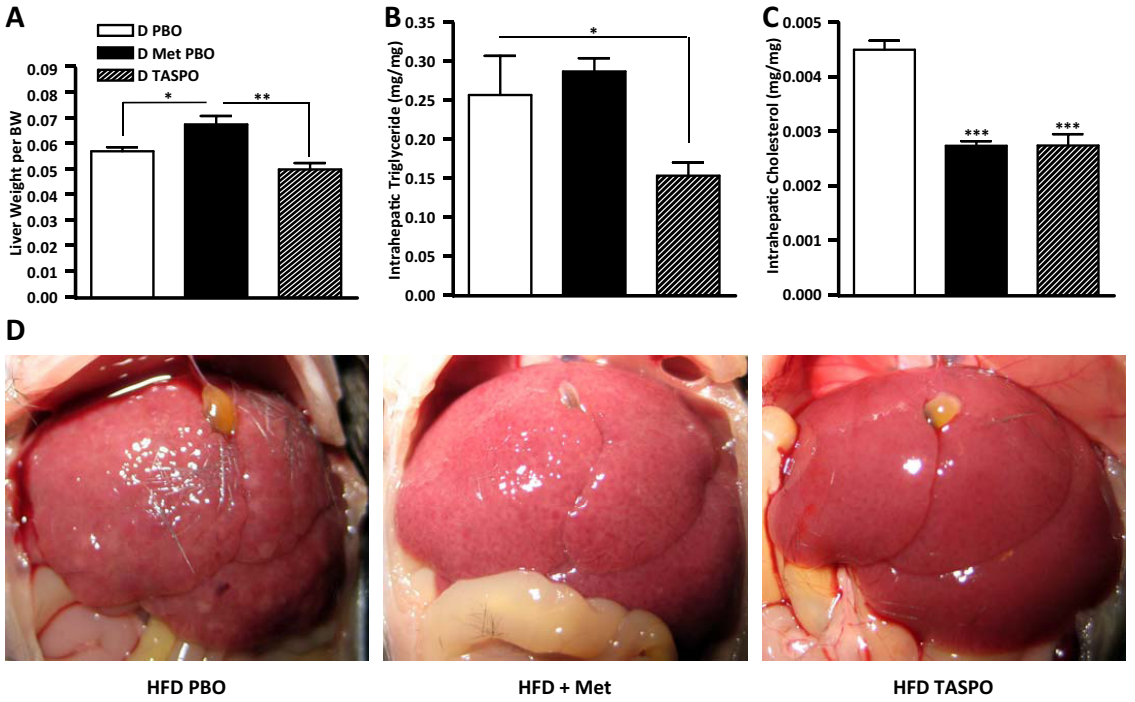

FIG. 3. Liver weights and lipid levels in diabetic *ApoE*$^{-/-}$ mice. Liver weights (panel A), triglycerides (panel B), cholesterol concentrations (panel C), and images of livers (panel D) after treatment of diabetic (D) *ApoE*$^{-/-}$ mice with vehicle alone (PBO), metformin (Met), or taspoglutide (TASPO). BW, Body weight; HFD, high-fat diet. *, $P < 0.05$; **, $P < 0.01$; ***, $P < 0.001$. Comparison between groups was made by one-way or two way ANOVA.

and *Abcg8* (Fig. 5, A–E), involved in cholesterol shuttling and clearance. The mRNA levels of *Lrp* were also increased after taspoglutide administration (Fig. 5F). In addition, the expression of the scavenger receptor (*Sr*) mRNA, involved in cholesterol-rich high-density lipoprotein and low-density lipoprotein uptake by hepatocytes, was also up-regulated in taspoglutide-treated mice (Fig. 5G). Taspoglutide also increased mRNA levels for hepatic lipase (*Lipc*), a key enzyme in the regulation of triglyceride storage and clearance (Fig. 5H), as well as *Cpt1a*, a rate-limiting mitochondrial fatty acid carrier regulating the rate of free fatty acid β-oxidation (Fig. 5I). Conversely, expression of *Fabp1*, *Fabp2*, and *Fatp5*, genes important for free fatty acid uptake and shuttling (Fig. 5, J–L), and perilipin (Fig. 5M), a marker of mature lipid droplets, was reduced in taspoglutide-treated livers. Taken together, these findings suggest that GLP-1R agonists induce a gene expression program favoring increased cholesterol, triglyceride, and fatty acid hepatic clearance and reducing the amount of free fatty acids taken up by hepatocytes.

Previous studies suggested that GLP-1R agonists control ectopic lipid deposition in part through direct activation of the native GLP-1R expressed on macrophages and hepatocytes (7, 31). Surprisingly however, we were unable to detect expression of *Glp1r* mRNA transcripts from macrophages isolated under a variety of conditions from three different lines of mice (wild-type C57BL/6, *ApoE*$^{-/-}$, and *IL10*$^{-/-}$); however, *Glp1r* mRNA transcripts were readily detected in RNA from murine islets, lung, and heart (Fig. 6A). Furthermore, although a weak signal corresponding to *Glp1r* mRNA transcripts was detected in RNA isolated from mouse liver, we did not detect a *Glp1r* mRNA transcript in RNA from isolated murine hepatocytes (Fig. 6A). Because several groups have reported

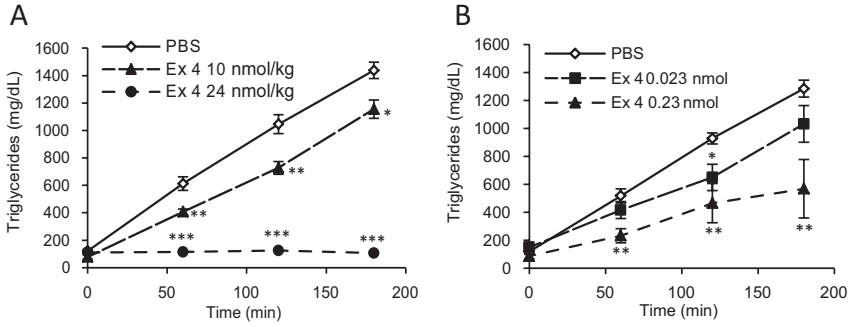

FIG. 4. Peripheral and central exendin-4 reduces hepatic triglyceride secretion. Plasma triglyceride levels were assessed as described in *Materials and Methods* in mice treated with various concentrations of exendin-4 administered by ip (A) or intracerebroventricular (B) injection. Data are mean ± SEM; n = 5-7. *, $P < 0.05$; **, $P < 0.01$; ***, $P < 0.001$ *vs.* PBS control

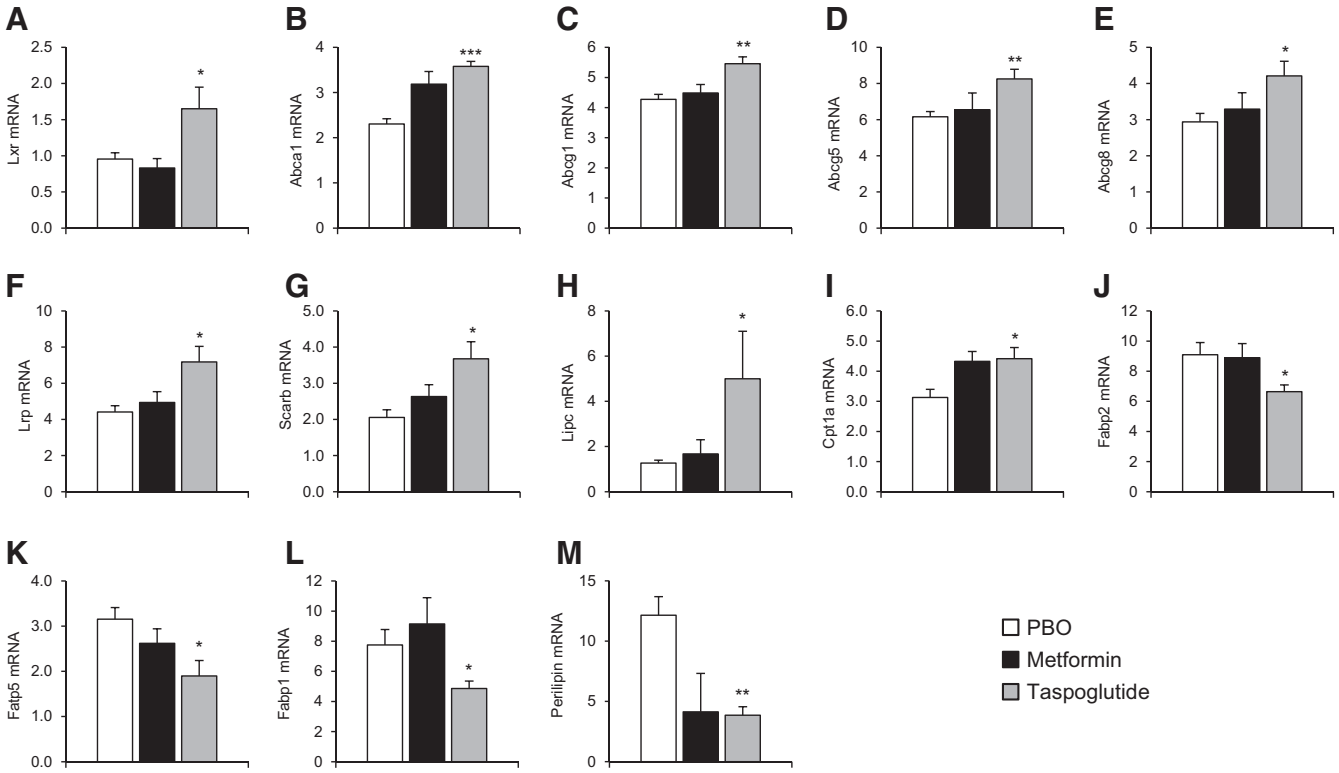

FIG. 5. Expression of genes controlling lipid metabolism in liver from diabetic *ApoE*$^{-/-}$ mice. Real-time PCR analysis was performed using RNA prepared from liver samples taken from random fed diabetic *ApoE*$^{-/-}$ mice at the end of the experiment outlined in Supplemental Fig. 1. A, *Lxr*; B, ATP-binding cassette subfamily A member 1 (*Abca1*); C, ATP-binding cassette sub-family G member 1 (*Abcg1*); D, ATP-binding cassette sub-family G member 5 (*Abcg5*); E, ATP-binding cassette subfamily G member 8 (*Abcg8*); F, Low density lipoprotein receptor-related protein (*Lrp*); G, scavenger receptor (*Sr*); H, hepatic lipase (*Lipc*); I, carnitine palmitoyltransferase 1a (*Cpt1a*); J, fatty acid binding protein 2 (*Fabp2*); K, solute carrier family 27 (fatty acid transporter), member 5 (*Fatp5*); L, fatty acid binding protein 1 (*Fabp1*); M, Perilipin. Results were normalized relative to levels of *Ppia* mRNA transcripts in the same samples. Data are mean ± SEM; n = 5. *, $P < 0.05$; **, $P < 0.01$; ***, $P < 0.001$ *vs.* placebo (PBO)-treated controls.

detection of an immunoreactive GLP-1R protein in macrophages and liver cells, we assessed the sensitivity and specificity of three different commercially available GLP-1R antisera commonly used to detect immunoreactive GLP-1R protein by Western blotting and/or immunocytochemistry. Remarkably, we were unable to verify that these antisera detect the native GLP-1R protein in conventional Western blot analysis using lung extracts from *Glp1r*$^{+/+}$ and *Glp1r*$^{-/-}$ mice (Fig. 6B), although the antisera did detect several immunoreactive bands ranging in size from approximately 54-65 kDa. To enhance the sensitivity of GLP-1R detection, protein extracts from mouse lung were first immunoprecipitated with one of two different GLP-1R antisera, after which immunoprecipitates were subjected to Western blot analysis with different GLP-1R antisera. Although multiple proteins ranging in size from approximately 54-96 kDa were detected (Fig. 6C), the number and relative abundance of proteins detected was comparable using lung extracts from *Glp1r*$^{+/+}$ and *Glp1r*$^{-/-}$ mice.

The results of these experiments suggested that these GLP-1R antisera were unable to detect the endogenous immunoreactive GLP-1R in murine tissues using conditions traditionally employed for conventional Western blot analysis. Accordingly, we transfected a C-terminal myc-His epitope-tagged murine GLP-1R cDNA into fibroblasts and repeated the experiments using extracts from transfected cells. Western blot analysis of whole-cell extracts did not detect the authentic immunoreactive GLP-1R protein, because identical immunoreactive bands were detected in cells transfected with the mouse GLP-1R cDNA or the cDNA expression vector pcDNA3.1/myc-His alone (Fig. 6D). In a further attempt to optimize the detection sensitivity of the GLP-1R antisera, we immunoprecipitated 500 μg protein extract from cells expressing a tagged transfected GLP-1R cDNA using an anti-Myc epitope antisera, followed by Western blot analysis with each of the three different GLP-1R antisera. We observed a very faint immunoreactive GLP-1R protein with two of the three GLP-1R antisera corresponding to the predicted size of the control transfected GLP-1R protein detected using an anti-His tag antisera (Fig. 6E). We next assessed whether immunoprecipitation with three different GLP-1R antisera followed by immunoblotting with an anti-c-myc antisera would detect a GLP-1R protein in BHK cells transfected with the mouse GLP-1R cDNA (Fig. 6F).

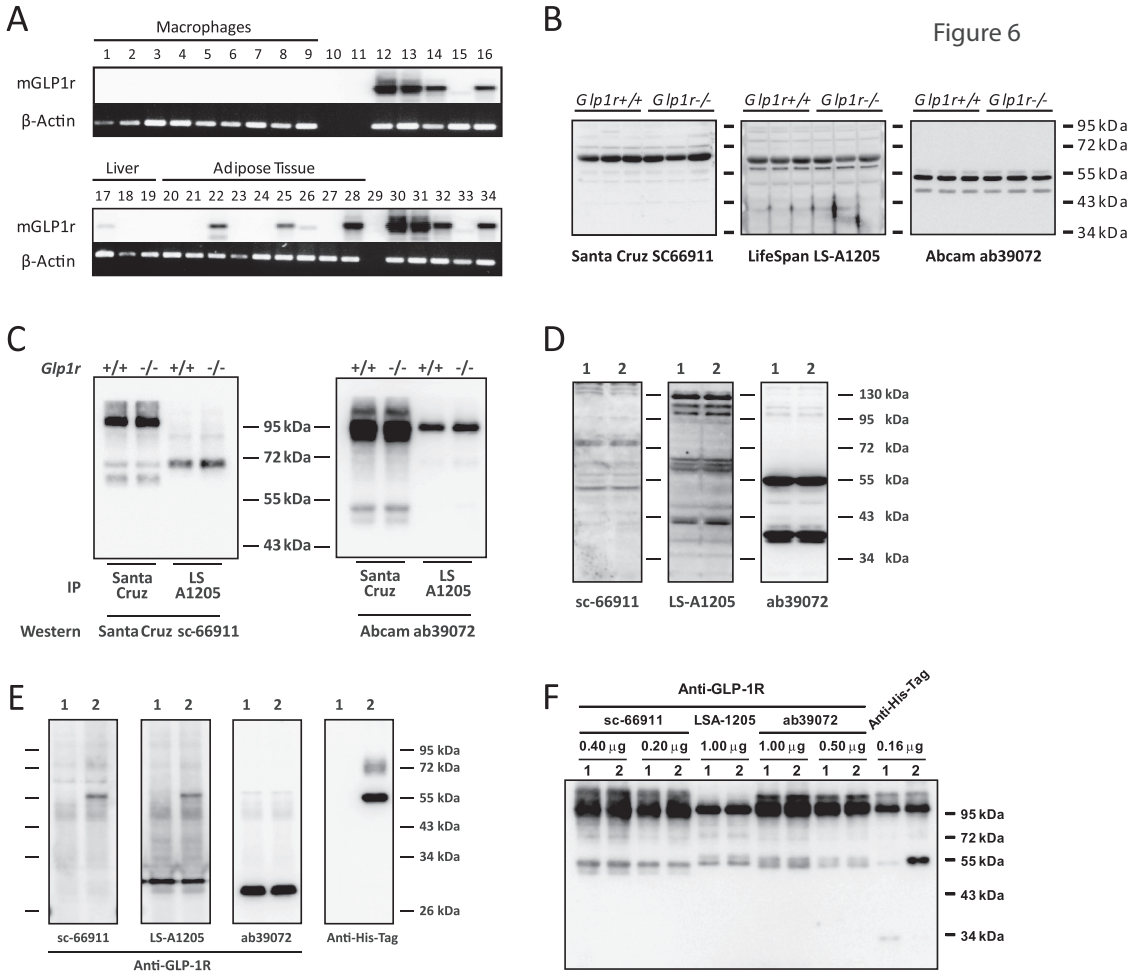

FIG. 6. Analysis of GLP-1R expression using PCR and Western blotting. A, Analysis of *Glp1r* and β-actin mRNA transcripts in isolated mouse macrophages, hepatocytes, and adipocytes by RT-PCR: lane 1, peritoneal macrophages; lane 2, peritoneal macrophages plated; lane 3, peritoneal macrophages 5 d after thioglycolate treatment, plated; lane 4, IL-10 $^{-/-}$ peritoneal macrophages, plated; lane 5, ApoE $^{-/-}$ peritoneal macrophages, plated; lane 6, FACS-sorted adipose tissue macrophages; lane 7, FACS-sorted peritoneal macrophages; lane 8, FACS-sorted peritoneal macrophages, sham; lane 9, FACS-sorted peritoneal macrophages, 160 nM PMA(Phorbol-12-myristate 13-acetate); lane 10, water; lane 11, blank; lane 12, pancreatic islets; lane 13, lung; lane 14, heart; lane 15, *Glp1r*$^{-/-}$ heart; lane 16, *Gipr*$^{-/-}$ heart; lane 17, liver; lane 18, hepatocytes; lane 19, nonhepatocyte liver fraction; lane 20, epididymal adipose tissue; lane 21, epididymal adipocytes; lane 22, epididymal stromal vascular fraction (SVF); lane 23, sc adipose tissue; lane 24, sc adipocytes; lane 25, sc SVF; lane 26, mesenteric adipose tissue; lane 27, mesenteric adipocytes; lane 28, mesenteric SVF; lane 29, water; lane 30, pancreatic islets; lane 31, lung; lane 32, heart; lane 33, *Glp1r* $^{-/-}$ heart; lane 34, *Gipr*$^{-/-}$ heart. All samples are from wild-type C57BL/6 mice, unless otherwise stated. B, Western blot analysis using whole tissue extracts prepared from lung tissue of three *Glp1r*$^{-/-}$ mice and three wild-type littermates. Blots were analyzed by immunoblotting with the indicated commercial GLP-1R antibodies. Molecular mass standards appear on the *right*. C, Whole-tissue extracts from lung of *Glp1r*$^{+/+}$ and *Glp1r*$^{-/-}$ mice after immunoprecipitation (IP) and Western blotting with the indicated commercial GLP-1R antibodies. D, BHK cells were transiently transfected with the vector pcDNA3.1/myc-His alone as a negative control (lane 1) or with the murine *Glp1r* cDNA cloned into pcDNA3.1/myc-His (lane 2). Whole-cell extracts (35 μg/lane protein) were prepared 48-72 h after transfection and analyzed by immunoblotting with the indicated GLP-1R antibodies. E and F, To enhance the sensitivity of detection, whole-cell extracts (500 μg protein) from transfected BHK cells (lane 1, control; lane 2, GLP-1R cDNA) were first immunoprecipitated either with Sepharose-conjugated anti-Myc-Tag antibody (E) or with the specified amounts (in micrograms) of commercial GLP-1R antibodies or anti-His-Tag antibody (F). Immune complexes were subsequently analyzed by Western blotting with the indicated antibodies (E) or with the mouse monoclonal anti-c-Myc (9E10) antiserum (F). The *far right lane* in E and F shows an immunoreactive GLP-1R protein of approximately 55 kDa.

Nevertheless, we were unable to detect any difference between control and GLP-1R-transfected cell extracts in this more sensitive immunoprecipitation/Western blot analysis. In contrast, immunoprecipitation of the GLP-1R protein using an anti-His antibody, followed by immunoblotting with the anti-myc antisera, readily detected expression of the GLP-1R protein in transfected fibroblasts.

Analysis of the targeting vector used to generate *Glp1r*$^{-/-}$ mice (15), together with characterization of *Glp1r* mRNA transcripts from *Glp1r*$^{-/-}$ islets, reveals that disruption of the *Glp1r* gene results in an internal deletion within the *Glp1r* coding sequence (32). We cloned *Glp1r* cDNAs from *Glp1r*$^{-/-}$ lung and intestine, and obtained two different sequences, designated the long and short *Glp1r*$^{-/-}$ cDNAs (Fig. 7, A and B). Sequence

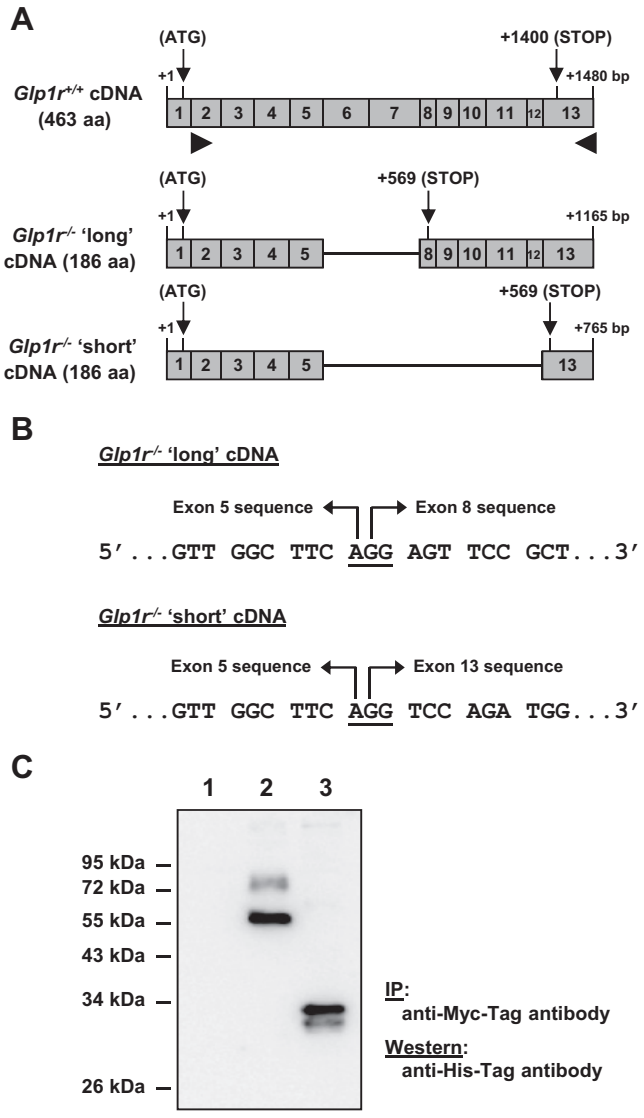

FIG. 7. A, Schematic representation of the *Glp1r* transcripts cloned from $Glp1r^{-/-}$ mouse tissue. Numbers 1-13 designate exons. The location of the translation start site (ATG, position +11) and stop codon are indicated for both the $Glp1r^{+/+}$ transcript and for the two $Glp1r^{-/-}$ cDNAs identified. The *arrowheads* mark the approximate position of the primers used for RT-PCR from lung and intestine RNA. The predicted size of the long and short $Glp1r^{-/-}$ cDNAs as well as the size of their encoded proteins are also indicated. B, Nucleotide sequence around the junction of exons 5 and 8 and exons 5 and 13 as observed in the long and short $Glp1r^{-/-}$ transcripts, respectively. *Underlined* is the codon where the predicted amino acid reading frame of each $Glp1r^{-/-}$ transcript is shifted, which creates an in-frame stop codon generating a carboxyl-terminal truncated GLP-1R protein. C, BHK cells were transiently transfected with the vector pcDNA3.1/myc-His alone (lane 1) or with the murine $Glp1r^{+/+}$ (lane 2) or $Glp1r^{-/-}$ long (lane 3) cDNAs cloned into pcDNA3.1/myc-His. Whole-cell extracts (500 μg protein) were immunoprecipitated with Sepharose-conjugated anti-Myc-Tag antibody, and the immune complexes were analyzed by Western blotting using anti-His-Tag antiserum.

analysis revealed internal deletion of exons 6 and 7 (long) or exons 6-12 (short), both of which encode a putative 186-amino-acid carboxyl-terminal truncated GLP-1R protein. Transfection of the cloned $Glp1r^{-/-}$ cDNA into BHK fibroblasts, followed by Western blot analysis using the anti-His antisera revealed a protein of less than 30 kDa, consistent with the $Glp1r^{-/-}$ cDNA sequence (Fig. 7, A and C). Hence, this much smaller GLP-1R-immunoreactive protein should be easily distinguished from the larger authentic GLP-1R when $Glp1r^{-/-}$ tissue extracts are used as controls in Western blot analyses.

Discussion

The available preclinical data demonstrate that GLP-1R agonists attenuate atherosclerosis progression (4). Continuous exendin-4 administration for 4 wk to young normoglycemic $ApoE^{-/-}$ mice fed standard rodent chow reduced macrophage adhesion to endothelial cells and aortic plaque and significantly decreased plaque area in the aortic sinus (7). Similarly, continuous administration of native GLP-1(7-36)amide for 4 wk reduced macrophage accumulation and aortic lesion size in young nondiabetic $ApoE^{-/-}$ mice, through mechanisms sensitive to the GLP-1R antagonist exendin(9-39) (10). Comparable antiatherogenic actions have been observed after administration of DPP-4 inhibitors to $ApoE^{-/-}$ mice, findings attributable to antiinflammatory actions of GLP-1R signaling in macrophages and endothelial cells (8, 33).

In contrast, our findings in high-fat-fed STZ-treated $ApoE^{-/-}$ mice differ substantially from previous reports in that we failed to detect evidence for GLP-1R-dependent reduction of lesion size in the thoracic or abdominal aorta. The lack of antiatherogenic activity in our studies may reflect the longer duration of treatment, the dose of taspoglutide used, the older age of mice, or the greater degree of hyperglycemia obtained after the combination of high-fat feeding and STZ. We intentionally selected doses of metformin and taspoglutide that produced glucoregulatory actions without producing substantial effects on food intake and body weight loss. It seems likely that treatment of mice with higher doses of these agents, leading to more profound weight loss, might enhance the antiatherogenic properties of antidiabetic agents. Nevertheless, our negative findings suggest that sustained GLP-1R activation, at levels sufficient to control blood glucose, does not universally lead to reduction of experimental atherosclerosis, and more work is clearly needed to understand the conditions and dose-response relationships required for coupling of GLP-1R activation to reduction of aortic plaque.

An equally unexpected finding was the lack of effect of taspoglutide on macrophage accumulation in the thoracic or abdominal aorta in $ApoE^{-/-}$ mice. The inflammatory state and migratory capacity of macrophages may be influenced by ambient levels of glucose, insulin, and free

fatty acids (5), and changes in these parameters in our diabetic $ApoE^{-/-}$ mice may have contributed to the failure of GLP-1R agonists to reduce macrophage adhesion to the aortic plaque or endothelium (11). Considerable evidence demonstrates that GLP-1R activation reduces lipid accumulation, attenuates endoplasmic reticulum stress, reduces macrophage migration, and decreases the expression of proinflammatory molecules in murine macrophages (7, 9, 10, 34-36). Nevertheless, we were unable to detect expression of the full-length *Glp1r* mRNA in peritoneal or adipose tissue macrophages isolated under various conditions from mice of multiple different genetic backgrounds. The majority of published studies assessing *Glp1r* mRNA expression in various cells and tissues such as macrophages rely predominantly on real-time PCR, which is highly sensitive but less specific relative to the detection of full-length *Glp1r* mRNA transcripts using techniques such as regular PCR and primers that enable detection of the entire GLP-1R coding sequence. Hence, although GLP-1R activation may indirectly control macrophage activation or migration, our data raise uncertainty about the direct actions of GLP-1R agonists on murine macrophages.

Characterization of several antisera commonly used to detect immunoreactive GLP-1R protein reveals that these antisera are not sufficiently sensitive to detect the native GLP-1R protein in cells or tissues using conditions routinely used for Western blot analysis. We selected lung extracts as a positive control for these experiments, because *Glp1r* expression has been reported to be relatively abundant in lung (Fig. 6) compared with other tissues (37). Furthermore, we were similarly unable to detect the GLP-1R protein with three different antisera in cells transfected with the GLP-1R cDNA, conditions favoring robust expression of the GLP-1R that is normally expressed at much lower levels in endogenous cells and tissues. Our experiments reveal that each of these antisera detect a number of nonspecific bands (evident in extracts from $Glp1r^{-/-}$ mice and cells transfected with the control pcDNA3.1/myc-His plasmid alone) of similar molecular size to the predicted immunoreactive GLP-1R. These findings raise a note of caution about interpretation of data generated using these antisera to detect GLP-1R expression in cell and tissue extracts and reemphasize the importance of appropriate controls in the interpretation of data obtained using the antisera.

The use of $Glp1r^{-/-}$ tissues as a control for assessing the sensitivity and specificity of GLP-1R antisera requires consideration of the possibility that under some circumstances, tissues from $Glp1r^{-/-}$ mice may express a smaller nonfunctional GLP-1R-immunoreactive protein that exhibits a molecular mass at least 20 kDa smaller than the authentic full-length GLP-1R protein (32). We have not been able to detect specific binding of GLP-1R agonists in tissues from $Glp1r^{-/-}$ mice (15), and we consistently fail to detect changes in glucose control, gastric emptying, or food intake in $Glp1r^{-/-}$ mice treated with potent GLP-1R agonists (15). It remains unclear whether a smaller truncated GLP-1R-immunoreactive protein potentially produced in $Glp1r^{-/-}$ mice is successfully transported from the endoplasmic reticulum to reach the cell membrane or, alternatively, whether it is subject to enhanced degradation in cell organelles in tissues of $Glp1r^{-/-}$ mice. Nevertheless, because the molecular size of the GLP-1R-immunoreactive protein predicted to be produced in $Glp1r^{-/-}$ mice is markedly smaller than the authentic GLP-1R, it should not be difficult to distinguish these proteins by Western blot analyses. The use of antisera for immunohistochemical detection of the GLP-1R is subject to the same cautions and concerns outlined for Western blot analyses and requires equally careful use of positive and negative controls.

Sustained GLP-1R activation reduces hepatic fat accumulation, and increased hepatic lipid oxidation, reduced lipogenesis, and enhanced lipoprotein secretion have been invoked as mechanisms contributing to reduced hepatic steatosis (27, 38-42). Chronic GLP-1R activation reduces hepatic very-low-density lipoprotein production in high-fat-fed mice (43), and acute intracerebroventricular administration of GLP-1 during hyperinsulinemic-euglycemic clamp experiments rapidly reduced hepatic triglyceride content in high-fat-fed mice (30). Nevertheless, we observed that acute exendin-4 administration via the intracerebroventricular or peripheral routes actually reduced triglyceride secretion into plasma of fasted mice, consistent with GLP-1R-dependent inhibition of hepatic lipid secretion. Our findings are in agreement with studies in high-fat-fed mice chronically infused with intracerebroventricular GLP-1 for 2 wk that also exhibited reduced plasma triglyceride levels under hyperinsulinemic-euglycemic conditions (44). Hence, GLP-1R activation is unlikely to reduce hepatic fat accumulation by promoting enhanced very-low-density lipoprotein secretion.

Review of changes in hepatic gene expression in $ApoE^{-/-}$ mice suggests that taspoglutide treatment decreases hepatic lipid storage via the stimulation of lipid clearance. The increase in mRNA transcripts for *Lxr* and *Lxr*-regulated genes *Abca1*, *Abcg1*, *Abcg5*, and *Abcg8* might contribute to the decrease in hepatic cholesterol content by increasing reverse cholesterol transport and excretion in bile in taspoglutide-treated mice. Furthermore, the increase in hepatic lipase and *Cpt1a* expression suggests an increased ratio of fatty acids targeted toward β-oxidation rather than triglyceride storage, consistent with previous findings (40, 45), whereas the decrease in

fatty acid transporters likely results in reduced hepatic fatty acid uptake and hepatocyte triglyceride storage. Although mechanisms through which GLP-1R activation controls hepatocyte lipid pathways and LXR remain unclear, one candidate may be insulin. Taspoglutide treatment increased basal insulin levels, and GLP-1R agonists may also enhance insulin sensitivity indirectly through weight loss. As insulin activates the LXR pathway (46), the role of insulin as a downstream target for the effects of GLP-1R agonists on hepatic lipid metabolism requires further investigation. Alternatively, GLP-1R agonists may also control hepatic lipid metabolism indirectly via reduced production of intestinal lipoproteins or changes in glucagon levels or via neuronal circuits, and the potential contributions of these mechanisms to GLP-1R-dependent reduction of hepatic fat require further investigation.

Nevertheless, despite experiments invoking a direct role for GLP-1R agonists on liver cells, *Glp1r* expression in hepatocytes remains controversial. *Glp1r* mRNA transcripts have been detected in human liver (38) by RT-PCR and an immunoreactive GLP-1R protein was detected in murine, rat, and human hepatocytes by Western blotting (31, 38, 41, 45). In contrast, other investigators have failed to detect mRNA transcripts encoding a full-length *Glp1r* in human, rat, or mouse liver (17, 37, 47-49), and we previously reported the absence of cAMP accumulation in response to GLP-1 or exendin-4 in isolated murine hepatocytes (17). Our current PCR analysis using primers that span nearly the entire *Glp1r* coding region failed to detect *Glp1r* expression in isolated murine hepatocytes, whereas the faint transcript in RNA isolated from whole liver is consistent with a signal emanating from blood vessels, bile ducts, neurons, or infiltrating immune cells within the liver. Hence, the reduction in liver fat in mice treated with GLP-1R agonists is not explained by a direct effect of GLP-1R signaling in hepatocytes.

In summary, our results raise several questions surrounding GLP-1 action, atherosclerosis, and hepatic fat accumulation. Our findings fail to demonstrate attenuation of atherosclerosis in either the thoracic or abdominal aorta of diabetic $ApoE^{-/-}$ mice. Furthermore, we did not observe reduced macrophage accumulation in the aorta after sustained GLP-1R activation, and we were unable to detect *Glp1r* mRNA transcripts in macrophages or hepatocytes, despite previous reports localizing the GLP-1R to these two cell types. Importantly, our findings reveal substantial problems with the sensitivity and specificity of multiple GLP-1R antisera commonly used for the detection of the GLP-1R in various tissues. Taken together, our findings emphasize the importance of additional experimentation to identify mechanisms and conditions linking GLP-1R activation to the control of macrophage migration, hepatocyte lipid metabolism, and ectopic lipid deposition.

Acknowledgments

We thank Wendy So for assistance with histology.

Address all correspondence and requests for reprints to: Dr. Daniel J. Drucker, Samuel Lunenfeld Research Institute, Mt. Sinai Hospital, 600 University Avenue TCP5-1004, Toronto Ontario Canada M5G 1X5. E-mail: d.drucker@utoronto.ca.

These studies were supported in part by a grant from Roche Inc. and by a grant from the Heart and Stroke Foundation of Ontario NA-6997. E.M. and J.C. are supported by fellowships from the Canadian Diabetes Association and the Canadian Institutes for Health Research, respectively. D.J.D. is supported in part by the Canada Research Chairs Program and a Banting and Best Diabetes Centre Novo Nordisk Chair in Incretin Biology.

D.J.D. is the guarantor of this work and, as such, had full access to all the data in the study and takes responsibility for the integrity of the data and the accuracy of the data analysis. N.P., E.M., C.L., T.B., J.C., L.B., X.C., C.S., D.H., and B.Y. carried out experiments and wrote and reviewed the paper. D.J.D. planned experiments, reviewed data, and wrote the paper.

Disclosure Summary: None of the authors have any conflicts of interest in regard to the experimental data presented herein.

References

1. **Inzucchi SE, Bergenstal RM, Buse JB, Diamant M, Ferrannini E, Nauck M, Peters AL, Tsapas A, Wender R, Matthews DR** 2012 Management of hyperglycemia in type 2 diabetes: a patient-centered approach: position statement of the American Diabetes Association (ADA) and the European Association for the Study of Diabetes (EASD). Diabetes Care 35:1364-1379
2. **Drucker DJ** 2006 The biology of incretin hormones. Cell Metab 3:153-165
3. **Noyan-Ashraf MH, Momen MA, Ban K, Sadi AM, Zhou YQ, Riazi AM, Baggio LL, Henkelman RM, Husain M, Drucker DJ** 2009 GLP-1R agonist liraglutide activates cytoprotective pathways and improves outcomes after experimental myocardial infarction in mice. Diabetes 58:975-983
4. **Ussher JR, Drucker DJ** 2012 Cardiovascular biology of the incretin system. Endocr Rev 33:187-215
5. **Sivertsen J, Rosenmeier J, Holst JJ, Vilsbøll T** 2012 The effect of glucagon-like peptide 1 on cardiovascular risk. Nat Rev Cardiol 9:209-222
6. **Drucker DJ, Goldfine AB** 2011 Cardiovascular safety and diabetes drug development. Lancet 11:977-979
7. **Arakawa M, Mita T, Azuma K, Ebato C, Goto H, Nomiyama T, Fujitani Y, Hirose T, Kawamori R, Watada H** 2010 Inhibition of monocyte adhesion to endothelial cells and attenuation of atherosclerotic lesion by a glucagon-like peptide-1 receptor agonist, exendin-4. Diabetes 59:1030-1037
8. **Matsubara J, Sugiyama S, Sugamura K, Nakamura T, Fujiwara Y, Akiyama E, Kurokawa H, Nozaki T, Ohba K, Konishi M, Maeda H, Izumiya Y, Kaikita K, Sumida H, Jinnouchi H, Matsui K, Kim-Mitsuyama S, Takeya M, Ogawa H** 2012 A dipeptidyl peptidase-4 inhibitor, des-fluoro-sitagliptin, improves endothelial function and

reduces atherosclerotic lesion formation in apolipoprotein E-deficient mice. J Am Coll Cardiol 59:265-276
9. **Vittone F, Liberman A, Vasic D, Ostertag R, Esser M, Walcher D, Ludwig A, Marx N, Burgmaier M** 2012 Sitagliptin reduces plaque macrophage content and stabilises arteriosclerotic lesions in *Apoe*$^{-/-}$ mice. Diabetologia 55:2267-2275
10. **Nagashima M, Watanabe T, Terasaki M, Tomoyasu M, Nohtomi K, Kim-Kaneyama J, Miyazaki A, Hirano T** 2011 Native incretins prevent the development of atherosclerotic lesions in apolipoprotein E knockout mice. Diabetologia 54:2649-2659
11. **Bornfeldt KE, Tabas I** 2011 Insulin resistance, hyperglycemia, and atherosclerosis. Cell Metab 14:575-585
12. **Maida A, Hansotia T, Longuet C, Seino Y, Drucker DJ** 2009 Differential importance of GIP versus GLP-1 receptor signaling for β-cell survival in mice. Gastroenterology 137:2146-2157
13. **Sauvé M, Ban K, Momen MA, Zhou YQ, Henkelman RM, Husain M, Drucker DJ** 2010 Genetic deletion or pharmacological inhibition of dipeptidyl peptidase-4 improves cardiovascular outcomes following myocardial infarction in mice. Diabetes 59:1063-1073
14. **Maida A, Lamont BJ, Cao X, Drucker DJ** 2011 Metformin regulates the incretin receptor axis via a pathway dependent on peroxisome proliferator-activated receptor-α in mice. Diabetologia 54:339-349
15. **Scrocchi LA, Brown TJ, MaClusky N, Brubaker PL, Auerbach AB, Joyner AL, Drucker DJ** 1996 Glucose intolerance but normal satiety in mice with a null mutation in the glucagon-like peptide receptor gene. Nature Med 2:1254-1258
16. **Hansotia T, Baggio LL, Delmeire D, Hinke SA, Yamada Y, Tsukiyama K, Seino Y, Holst JJ, Schuit F, Drucker DJ** 2004 Double incretin receptor knockout (DIRKO) mice reveal an essential role for the enteroinsular axis in transducing the glucoregulatory actions of DPP-IV inhibitors. Diabetes 53:1326-1335
17. **Flock G, Baggio LL, Longuet C, Drucker DJ** 2007 Incretin receptors for glucagon-like peptide 1 and glucose-dependent insulinotropic polypeptide are essential for the sustained metabolic actions of vildagliptin in mice. Diabetes 56:3006-3013
18. **Rodbell M** 1964 Metabolism of isolated fat cells. I. Effects of hormones on glucose metabolism and lipolysis. J Biol Chem 239:375-380
19. **Hadjiyanni I, Baggio LL, Poussier P, Drucker DJ** 2008 Exendin-4 modulates diabetes onset in nonobese diabetic mice. Endocrinology 149:1338-1349
20. **Yusta B, Baggio LL, Estall JL, Koehler JA, Holland DP, Li H, Pipeleers D, Ling Z, Drucker DJ** 2006 GLP-1 receptor activation improves β-cell function and survival following induction of endoplasmic reticulum stress. Cell Metab 4:391-406
21. **Baggio LL, Huang Q, Brown TJ, Drucker DJ** 2004 A recombinant human glucagon-like peptide (GLP)-1-albumin protein (albugon) mimics peptidergic activation of GLP-1 receptor-dependent pathways coupled with satiety, gastrointestinal motility, and glucose homeostasis. Diabetes 53:2492-2500
22. **Lamont BJ, Li Y, Kwan E, Brown TJ, Gaisano H, Drucker DJ** 2012 Pancreatic GLP-1 receptor activation is sufficient for incretin control of glucose metabolism in mice. J Clin Invest 122:388-402
23. **Hsieh J, Longuet C, Baker CL, Qin B, Federico LM, Drucker DJ, Adeli K** 2010 The glucagon-like peptide 1 receptor is essential for postprandial lipoprotein synthesis and secretion. Diabetologia 53: 552-561
24. **Daugherty A, Whitman SC** 2003 Quantification of atherosclerosis in mice. Methods Mol Biol 209:293-309
25. **Kleiner DE, Brunt EM, Van Natta M, Behling C, Contos MJ, Cummings OW, Ferrell LD, Liu YC, Torbenson MS, Unalp-Arida A, Yeh M, McCullough AJ, Sanyal AJ** 2005 Design and validation of a histological scoring system for nonalcoholic fatty liver disease. Hepatology 41:1313-1321
26. **Sebokova E, Christ AD, Wang H, Sewing S, Dong JZ, Taylor J, Cawthorne MA, Culler MD** 2010 Taspoglutide, an analog of human glucagon-like peptide-1 with enhanced stability and in vivo potency. Endocrinology 151:2474-2482
27. **Mells JE, Fu PP, Sharma S, Olson D, Cheng L, Handy JA, Saxena NK, Sorescu D, Anania FA** 2012 GLP-1 analogue, liraglutide ameliorates hepatic steatosis and cardiac hypertrophy in C57BL/6J mice fed a western diet. Am J Physiol Gastrointest Liver Physiol 302: G225–G335
28. **Samson SL, Sathyanarayana P, Jogi M, Gonzalez EV, Gutierrez A, Krishnamurthy R, Muthupillai R, Chan L, Bajaj M** 2011 Exenatide decreases hepatic fibroblast growth factor 21 resistance in non-alcoholic fatty liver disease in a mouse model of obesity and in a randomised controlled trial. Diabetologia 54:3093-3100
29. **Baggio LL, Huang Q, Cao X, Drucker DJ** 2008 The long-acting albumin-exendin-4 GLP-1R agonist CJC-1134 engages central and peripheral mechanisms regulating glucose homeostasis. Gastroenterology 134:1137-1147
30. **Burmeister MA, Ferre T, Ayala JE, King EM, Holt RM, Ayala JE** 2012 Acute activation of central GLP-1 receptors enhances hepatic insulin action and insulin secretion in high-fat-fed, insulin resistant mice. Am J Physiol Endocrinol Metab 302:E334–E343
31. **Gupta NA, Mells J, Dunham RM, Grakoui A, Handy J, Saxena NK, Anania FA** 2010 Glucagon-like peptide-1 receptor is present on human hepatocytes and has a direct role in decreasing hepatic steatosis in vitro by modulating elements of the insulin signaling pathway. Hepatology 51:1584-1592
32. **Flamez D, Van Breusegem A, Scrocchi LA, Quartier E, Pipeleers D, Drucker DJ, Schuit F** 1998 Mouse pancreatic β-cells exhibit preserved glucose competence after disruption of the glucagon-like peptide 1 receptor gene. Diabetes 47:646-652
33. **Terasaki M, Nagashima M, Watanabe T, Nohtomi K, Mori Y, Miyazaki A, Hirano T** 2012 Effects of PKF275-055, a dipeptidyl peptidase-4 inhibitor, on the development of atherosclerotic lesions in apolipoprotein E-null mice. Metabolism 61:974-977
34. **Liang CP, Han S, Li G, Tabas I, Tall AR** 2012 Impaired MEK signaling and SERCA expression promote ER stress and apoptosis in insulin-resistant macrophages and are reversed by exenatide treatment. Diabetes 61:2609-2620
35. **Lee YS, Park MS, Choung JS, Kim SS, Oh HH, Choi CS, Ha SY, Kang Y, Kim Y, Jun HS** 2012 Glucagon-like peptide-1 inhibits adipose tissue macrophage infiltration and inflammation in an obese mouse model of diabetes. Diabetologia 55:2456-2468
36. **Kodera R, Shikata K, Kataoka HU, Takatsuka T, Miyamoto S, Sasaki M, Kajitani N, Nishishita S, Sarai K, Hirota D, Sato C, Ogawa D, Makino H** 2011 Glucagon-like peptide-1 receptor agonist ameliorates renal injury through its anti-inflammatory action without lowering blood glucose level in a rat model of type 1 diabetes. Diabetologia 54:965-978
37. **Bullock BP, Heller RS, Habener JF** 1996 Tissue distribution of messenger ribonucleic acid encoding the rat glucagon-like peptide 1 receptor. Endocrinology 137:2968-2978
38. **Svegliati-Baroni G, Saccomanno S, Rychlicki C, Agostinelli L, De Minicis S, Candelaresi C, Faraci G, Pacetti D, Vivarelli M, Nicolini D, Garelli P, Casini A, Manco M, Mingrone G, Risaliti A, Frega GN, Benedetti A, Gastaldelli A** 2011 Glucagon-like peptide-1 receptor activation stimulates hepatic lipid oxidation and restores hepatic signalling alteration induced by a high-fat diet in nonalcoholic steatohepatitis. Liver Int 31:1285-1297
39. **Sharma S, Mells JE, Fu PP, Saxena NK, Anania FA** 2011 GLP-1 analogs reduce hepatocyte steatosis and improve survival by enhancing the unfolded protein response and promoting macroautophagy. PLoS One 6:e25269
40. **Ben-Shlomo S, Zvibel I, Shnell M, Shlomai A, Chepurko E, Halpern Z, Barzilai N, Oren R, Fishman S** 2011 Glucagon-like peptide-1 reduces hepatic lipogenesis via activation of AMP-activated protein kinase. J Hepatol 54:1214-1223
41. **Lee J, Hong SW, Chae SW, Kim DH, Choi JH, Bae JC, Park SE, Rhee EJ, Park CY, Oh KW, Park SW, Kim SW, Lee WY** 2012 Exendin-4

improves steatohepatitis by increasing Sirt1 expression in high-fat diet-induced obese C57BL/6J mice. PLoS One 7:e31394
42. **Trevaskis JL, Griffin PS, Wittmer C, Neuschwander-Tetri BA, Brunt EM, Dolman CS, Erickson MR, Napora J, Parkes DG, Roth JD** 2012 Glucagon-like peptide-1 receptor agonism improves metabolic, biochemical, and histopathological indices of nonalcoholic steatohepatitis in mice. Am J Physiol Gastrointest Liver Physiol 302: G762–G772
43. **Parlevliet ET, Schröder-van der Elst JP, Corssmit EP, Picha K, O'Neil K, Stojanovic-Susulic V, Ort T, Havekes LM, Romijn JA, Pijl H** 2009 CNTO736, a novel glucagon-like peptide-1 receptor agonist, ameliorates insulin resistance and inhibits very low-density lipoprotein production in high-fat-fed mice. J Pharmacol Exp Ther 328:240-248
44. **Parlevliet ET, de Leeuw van Weenen JE, Romijn JA, Pijl H** 2010 GLP-1 treatment reduces endogenous insulin resistance via activation of central GLP-1 receptors in mice fed a high-fat diet. Am J Physiol Endocrinol Metab 299:E318–E324
45. **Ding X, Saxena NK, Lin S, Gupta NA, Gupta N, Anania FA** 2006 Exendin-4, a glucagon-like protein-1 (GLP-1) receptor agonist, reverses hepatic steatosis in ob/ob mice. Hepatology 43:173-181
46. **Kalaany NY, Gauthier KC, Zavacki AM, Mammen PP, Kitazume T, Peterson JA, Horton JD, Garry DJ, Bianco AC, Mangelsdorf DJ** 2005 LXRs regulate the balance between fat storage and oxidation. Cell Metab 1:231-244
47. **Aviv V, Meivar-Levy I, Rachmut IH, Rubinek T, Mor E, Ferber S** 2009 Exendin-4 promotes liver cell proliferation and enhances the PDX-1-induced liver to pancreas transdifferentiation process. J Biol Chem 284:33509-33520
48. **Dunphy JL, Taylor RG, Fuller PJ** 1998 Tissue distribution of rat glucagon receptor and GLP-1 receptor gene expression. Mol Cell Endocrinol 141:179-186
49. **Tomas E, Stanojevic V, Habener JF** 2010 GLP-1 (9-36) amide metabolite suppression of glucose production in isolated mouse hepatocytes. Horm Metab Res 42:657-662

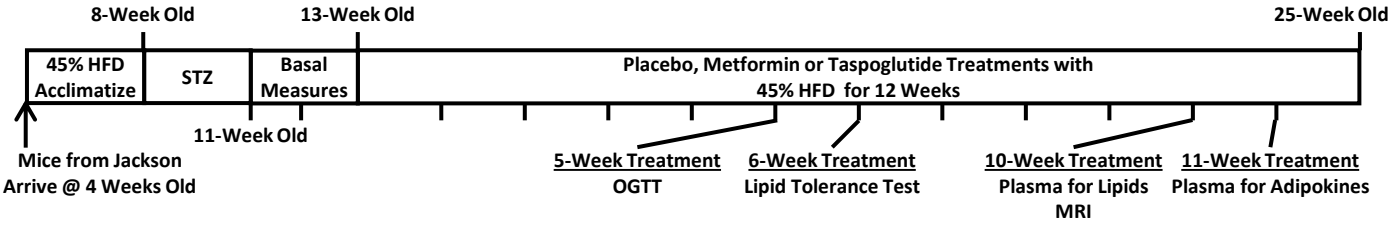

Supplementary Figure 1 Experimental timelines for analysis of atherosclerosis in *ApoE*-/- mice

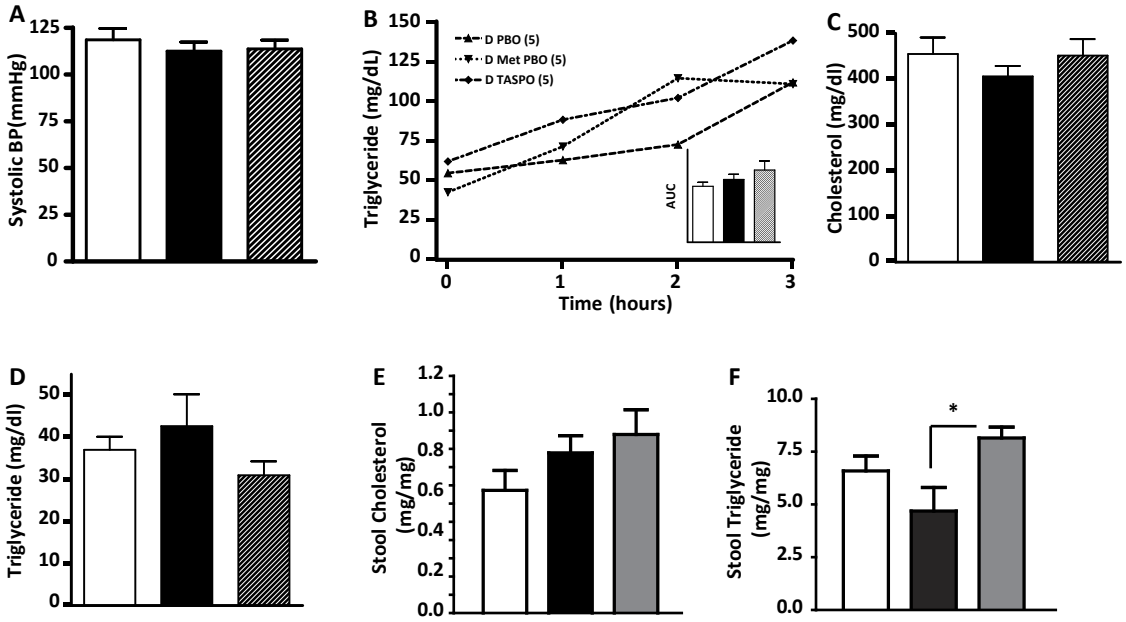

Supplementary Figure 2. Plasma and stool lipid levels in diabetic male ApoE-/- mice. (A) Blood pressure (B) Plasma triglyceride levels measured after oral olive oil administration in different groups of ApoE-/- mice. Fasting (6-hour) plasma levels of (C) cholesterol and (D) triglycerides after 11 weeks of treatment and levels of excreted cholesterol (E) and triglycerides (F) in stool from different groups of ApoE-/- mice. Analysis of lipid tolerance graph was made by two-way ANOVA and AUC by one-way ANOVA.

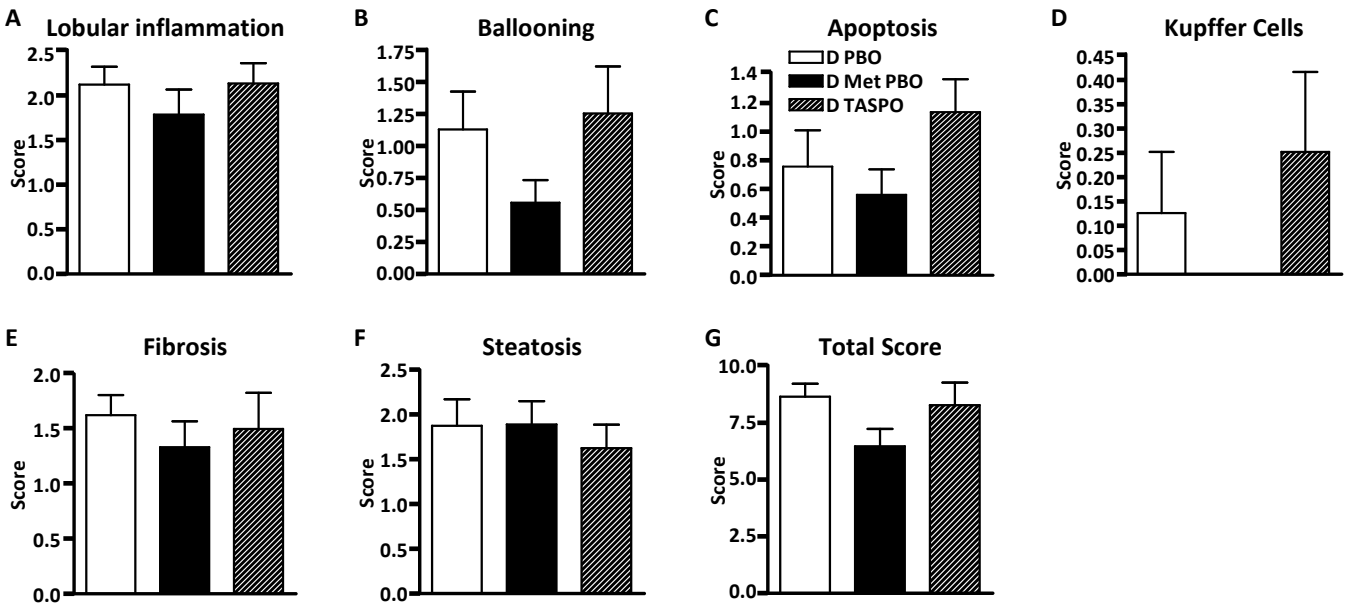

Supplementary Figure 3. Histological indices of liver injury in diabetic *ApoE*-/- mice after 12 weeks of treatment. Analysis of NAFLD activity scores (NAS) for hepatic lobular inflammation, ballooning, apoptosis, Kupffer cells, fibrosis and steatosis were assessed by a pathologist blinded to the study. D PBO= diabetic placebo, D Met PBO = diabetic mice treated with metformin and a "placebo" microtablet and D Taspo = diabetic mice treated with taspoglutide.

	Diabetic PBO		Diabetic Taspo				Diabetic Met				
	Average	SEM	Average	SEM	Fold over PBO	p value vs D PBO	Average	SEM	Fold over PBO	p value vs D PBO	p value vs taspo
Transcription factors											
Foxa2	2.74	± 0.26	2.82	± 0.44	1.03	0.7965	2.30	± 0.15	0.84	0.0415	0.2936
SREBP1	2.85	± 0.51	3.17	± 0.32	1.11	0.7063	3.09	± 0.64	1.08	0.8699	0.9075
srebp2	1.03	± 0.12	0.98	± 0.10	0.95	0.8843	1.05	± 0.16	1.02	0.8163	0.7158
PPARa	1.27	± 0.14	1.31	± 0.17	1.03	0.8239	1.57	± 0.26	1.24	0.5503	0.4256
Beta oxidation											
ACoAOxidase	1.89	± 0.16	1.77	± 0.13	0.93	0.5511	2.49	± 0.32	1.31	0.2000	0.0729
Cpt2	7.23	± 0.60	7.18	± 0.38	0.99	0.6691	8.33	± 0.92	1.15	0.5150	0.2822
Lipid uptake											
FATP2	9.18	± 1.77	8.66	± 1.14	0.94	0.8101	10.39	± 1.18	1.13	0.5844	0.3201
FABP5	1.30	± 0.13	1.48	± 0.25	1.14	0.5490	1.31	± 0.11	1.00	0.9866	0.5459
CD36	2.32	± 0.18	2.33	± 0.19	1.00	0.9761	2.38	± 0.21	1.03	0.8361	0.8601
LDLR	1.36	± 0.12	1.39	± 0.15	1.02	0.8837	1.43	± 0.22	1.05	0.8091	0.9018
Lipoprotein assembly											
DGAT1	3.17	+ 0.15	2.58	+ 0.22	0.81	0.0557	2.85	+ 0.15	0.90	0.1717	0.3244
DGAT2	4.86	± 0.43	4.85	± 0.49	1.00	0.9968	5.04	± 0.69	1.04	0.8299	0.8332
MTTP	2.75	± 0.22	2.63	± 0.24	0.96	0.7197	2.71	± 0.28	0.99	0.9274	0.8207
LPL	2.00	+ 0.21	2.69	+ 0.51	1.35	0.2394	2.09	± 0.15	1.05	0.7143	0.2900
ApoA5	1.18	± 0.18	1.06	± 0.05	0.90	0.5254	1.34	± 0.14	1.13	0.5006	0.0939
ApoB	7.13	± 0.43	6.56	± 0.45	0.92	0.3787	7.34	± 0.50	1.03	0.7571	0.2723
ApoC3	6.89	± 0.47	6.16	± 0.51	0.89	0.3238	6.44	± 0.44	0.93	0.5026	0.6939
Cholesterol and bile acid synthesis											
HMGCoAR	6.70	± 0.82	5.56	± 0.99	0.83	0.7015	5.46	± 0.93	0.82	0.6439	0.9457
Cyp7a1	1.56	± 0.09	1.82	± 0.38	1.16	0.5820	1.63	± 0.42	1.04	0.9452	0.7414

Supplementary Table 1 Gene expression in liver of diabetic ApoE-/- mice

cDNA preparation and real time PCR analysis were performed as described in methods from whole liver samples taken from random fed diabetic ApoE-/- mice . Data are mean ± SEM, n=5. Diabetic PBO=diabetic ApoE-/- mice treated with placebo; Diabetic Taspo = mice treated with taspoglutide and Diabetic Met = mice treated with metformin, all for 12 weeks.

Supplementary Table 2

Primers used for Real Time PCR experiments described in Figure 5 and Supplementary Table 1

Figure 5

lxr	Mm00437262_m1
abca1	Mm00442646_m1
abcg1	Mm00437390_m1
abcg5	Mm00446241_m1
abcg8	Mm00445970_m1
lrp	Mm00464608_m1
SR	mm00450234
lipc	Mm00433975_m1
cpt1a	Mm01231183_m1
fabp2	Mm00433188
fatp5	Mm00447768_m1
fabp1	Mm00444340_m1
perilippin	Mm00558672_m1

Supplemental Table 1

foxa2	Mm01976556
srebp1	Mm00550338_m1
srebp2	Mm01306292_m1
ppara	Mm00627559
acoaoxidase	Mm00443579
cpt2	Mm00487205_m1
fatp2	Mm00449517_m1
fabp5	Mm00783731
cd36	Mm00432403
ldlr	Mm00440169_m1
dgat1	Mm00515643_m1
dgat2	Mm01273905_m1
mttp	Mm00435015
lpl	Mm00434770
apoa5	Mm00475480
apob	Mm01545059
apoc3	Mm00445670
hmgcoar	Mm01282499
cyp7a1	Mm00484152_m1